Terrain Shadow Detection from RapidEye Images Based on Hillshade Algorithm

Hyeonggyu Kim[1], Taejung Kim[1], Joongbin Lim[2] and Kyoung-Min Kim[2]
[1] Dept. Of Geoinformatic Engineering, Inha University, 100 Inha-ro, Michuhol-gu, Incheon 222112, Republic of Korea,
[2] Forest ICT Research Center, National Institute of Forest Science, 57 Hoegi-ro, Dongdaemun-gu, Seoul 02455, Republic of Korea,
Email: 22221164@inha.edu, tezid@inha.ac.kr, jlim@korea.kr, greenann@korea.kr

KEY WORDS: Terrain Shadow Detection, Hillshade Algorithm, DEM

ABSTRACT: To enable quick and ease utilization of satellite imagery, preprocessing of satellite imagery is necessary. Pixels that hinder accurate analysis should be identified and masked out. Such pixels include shadows. They disturb the irradiance from the actual earth surface and create confusion for dark objects such as water. In mountainous areas, terrain shadow occurs as a result of the terrain relief effect. It leads to accuracy in the analysis of change detection, classification, and other indices like NDVI. In this paper, we developed an automated technique to detect terrain shadow from satellite images at a 5m Ground Sampling Distance. A hillshade algorithm takes into account the sun's elevation and azimuth angles and the surface's slope and aspect angles to produce realistic terrain shadow effects. we demonstrated this algorithm could be applied to detect terrain shadows present in satellite imagery and to mask out shadow pixels accurately. To test the proposed method, the analysis was performed on mountainous areas using RapidEye images. Geometric and orthogonal corrections were applied to the satellite images. The sun's elevation and azimuth angles were prepared from the metadata of the satellite images used. The surface's slope and aspect angles were estimated from a Digital Elevation Model generated by the National Geographic Information Institute of Korea. The vectors for sun illumination direction and surface normal were then calculated. Shadow pixels were determined by calculating the angle between the two vectors and checking whether the angle exceeded 90 degrees. We then compared the predicted shadow pixels with the ground truth data. As a result, the overall accuracy of the prediction results was found to be greater than 85%. We conclude that our proposed method appears to be suitable for detecting terrain shadows.

1. INTRODUCTION

Commercial satellite services are expanding in the global satellite market due to the rapid rise of private participation, and the importance of satellite images utilization is emerging. Meanwhile, users who are unfamiliar with using satellite images have difficulty in processing satellite images. Thus, for convenient analysis of satellite images, it is essential to provide preprocessed data.

In land remote sensing, clouds or shadows obscure the analysis target and cause inaccurate analysis results. These pixels should be masked out or identified. Shadows disturb the irradiance from the actual Earth's surface and create confusion for dark objects such as water (Li *et al*., 2016; Shahtahmassebi, 2013). In mountainous regions, terrain shadow occurs as a result of the terrain relief effect. It leads to inaccurate accuracy in the field of remote sensing. As a result, many researchers have experimented for shadow detection methods (Tsai, 2006; Lorenzi *et al*., 2012; Zhang *et al*., 2014; Wang and Yan, 2016). We selected a geometric modeling approach, which is a detection methodology through the geometrical relationship between the Sun and the Earth's surface. Among the modeling approaches, we selected the hillshade algorithm. This algorithm takes into account the Sun's elevation, azimuth angle, and the surface's slope, and aspect angle to produce the terrain effect.

In paper, we experimented with terrain shadow detection using a Digital Elevation Model (DEM) was in rugged mountainous regions using Rapideye images. The DEM used for analysis was produced by the National Geographic Information Institute of Korea. The azimuth and elevation angles of the Sun were calculated in the algorithm through the image metadata. The height gradient of the DEM was estimated, and the slope and aspect angles of the Earth's surface were calculated. We estimated the directional vector of the Sun and the normal vector of the Earth's surface. When the angle between the two vectors exceeded 90 degrees, it was estimated as terrain shadows. We compared the proposed algorithm's results over three test regions with Ground Truth data. All three regions showed an overall accuracy of more than 85%.

2. USED DATA

We set up a test area in Hamheung-si in North Korea from a RapidEye image, and the A, B, and C regions were mainly set as the mountainous terrain. Figure 1 shows the entire research area (a), a DEM in hamheung (b). From Figure 1 (c) to 1(h), enlarged satellite images and DEMs over the test region A, B, C are shown. Table 1 shows the specifications of DEM data and the satellite image.

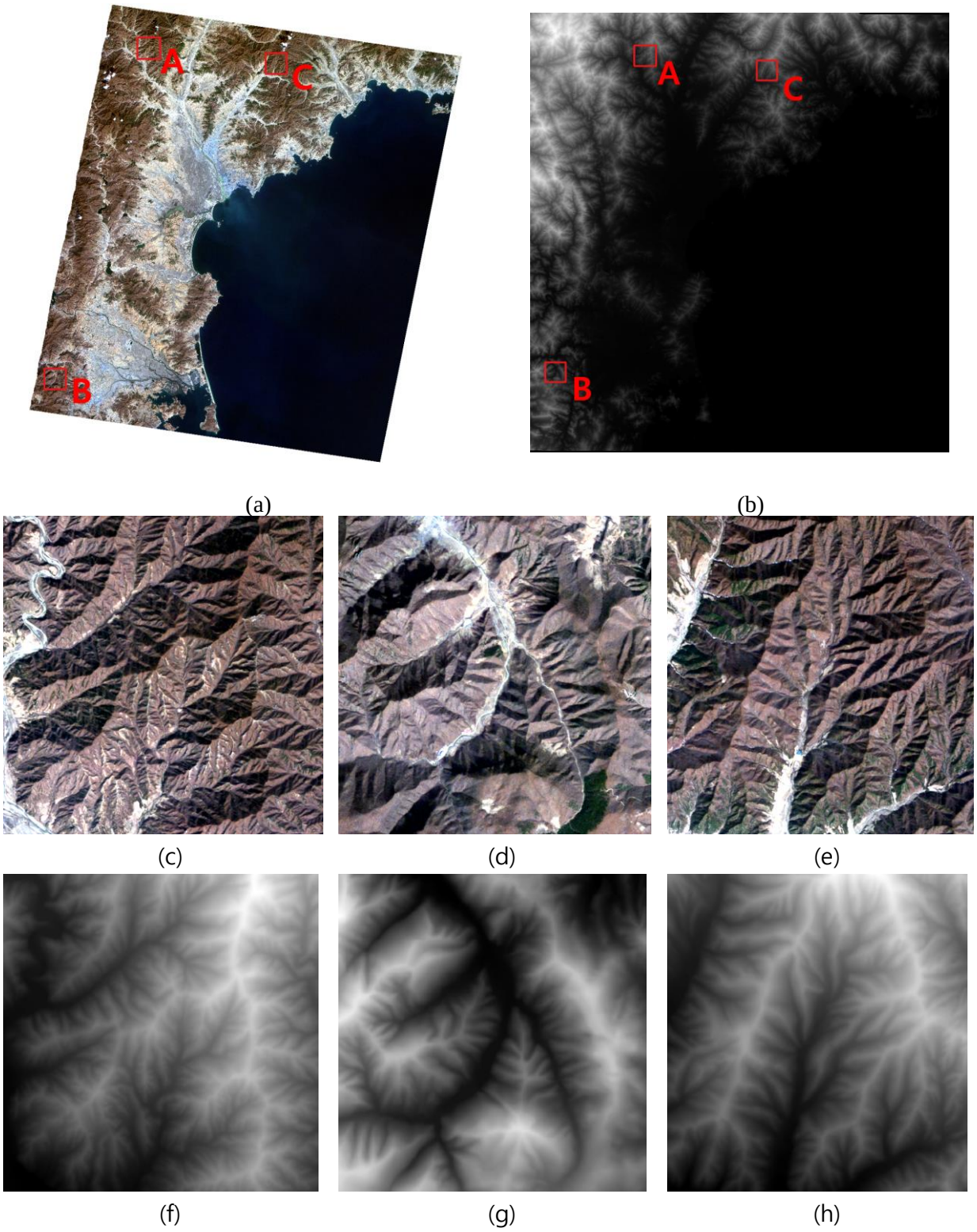

Figure 1. Study Area for detecting terrain shadows (a) Satellite Image used, (b) a DEM, (c) enlarge image over A region, (d) over B region, (e) over C region, (f) Dem over A region, (g) B region, and (h) C region.

Table 1. Specification of DEM and RapidEye Satellite Image

Data	DEM	Data	RapidEye L1B
Coordinate system	Transverse Mercator	Coordinate system	UTM-K
Spatial Resolution	10m	Spatial Resolution	5m
Data format	Img, ige	Data format	tif, xml(metadata)

3. METHODOLOGY

Figure 2 shows our proposed terrain shadow detection method. In this study, geometric correction and orthogonal correction of satellite images first were performed. And then, the Sun's azimuth and elevation angles were prepared. A DEM data was reprojected into the same coordinate system as the RapidEye images. From the reprojected Dem, we calculated the height gradients, dz/dx and dz/dy. Next, the slope and aspect angle of the surface were calculated. We applied the hillshade algorithm to the slope, aspect angles and the Sun's azimuth and elevation angles. Terrain shadows were then extracted. We assessed the accuracy of terrain shadow detection through comparison between Ground Truth and the extracted result.

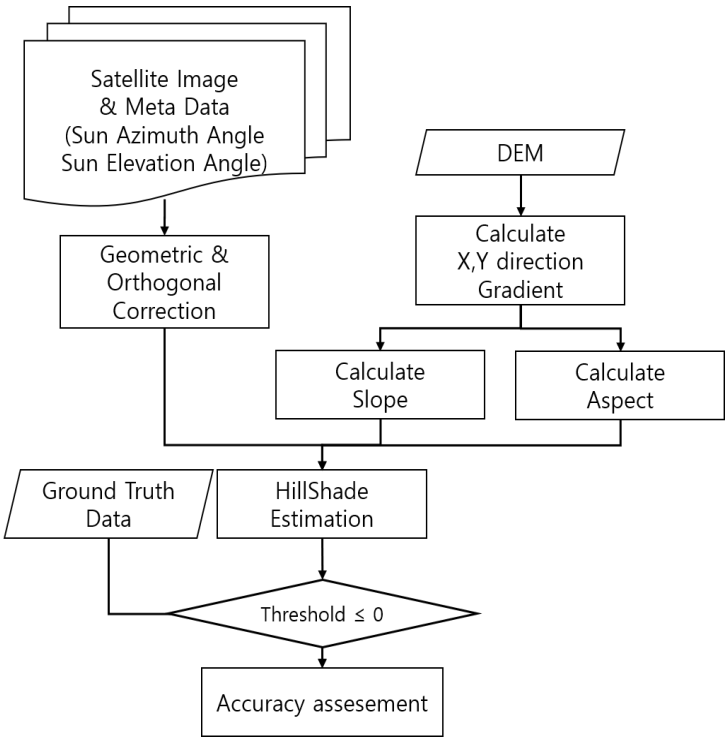

Figure 2. A flow chart of a proposed method

3.1 Preprocessing of meta data and input data

The RapidEye L1B image used in the study area requires geometric correction and orthogonal correction preprocessing. Therefore, orthocorrected images were created by performing geometric correction and orthogonal correction. In addition, the DEM data was reprojected from the TM coordinate system to the UTM-K coordinate system for matching satellite images. And it was resampled using Bilinear Interpolation with a spatial resolution like RapidEye images. We collected the Sun's elevation and azimuth angles at the image acquisition time from the image metadata. The Sun's azimuth angles were converted to the angle with the x-axis of the orthocorrected image for later calculation.

3.2 Gradient estimation of x-direction and y-direction

Gradient estimation equations in the X and Y axis direction are shown in equations (1), and (2) below. Dx and Dy are variation values obtained by estimating the rate of the Z value change expressed in a DEM in the X direction and Y direction. There are several techniques for gradient estimation, of which the Weighted Average Gradient method produced by Horn (1981) was used here. According to Figure 3, the equation by Horn was weighted twice as much as diagonal pixels with the weight of adjacent pixels based on Z(i,j) because if there was an error in the pixel value, it did not significantly affect the gradient estimation. Δx, Δy mean ground sample distance (GSD) or pixel size in x and y direction, respectively.

$Z_{i-1,j-1}$	$Z_{i-1,j}$	$Z_{i-1,j+1}$
$Z_{i,j-1}$	$Z_{i,j}$	$Z_{i,j+1}$
$Z_{i+1,j-1}$	$Z_{i+1,j}$	$Z_{i+1,j+1}$

Figure 3. Moving Window of 3 by 3 kernel

$$\frac{dz}{dx} = \frac{(Z_{i-1,j+1}+2Z_{i,j+1}+Z_{i+1,j+1})-(Z_{i-1,j-1}+2Z_{i,j-1}+Z_{i+1,j-1})}{8\times\Delta x} \quad (1)$$

$$\frac{dz}{dy} = \frac{(Z_{i+1,j-1}+2Z_{i+1,j}+Z_{i+1,j+1})-(Z_{i-1,j-1}+2Z_{i-1,j}+Z_{i-1,j+1})}{8\times\Delta y} \quad (2)$$

3.3 Create slope and aspect angle calculation

The slope angle is one of the representative characteristics of the terrain. It means the inclination angle of the surface on the horizon. The following equation (3) shows the equation of slope angle. The inclination angle was measured by squared the amount of change in the value from the corresponding pixel to the adjacent pixel. Z-factor is a correction factor adjusted when the unit of height value and the unit of axial direction are different. The default value for the Z-factor is 1. Our process uses 4 times of Z-factor. Figure 4 shows the relationship between the slope angle and normal vector on horizontal plane.

$$Slope = tan^{-1}\left(Z - factor * \sqrt{(\frac{dz}{dx})^2 + (\frac{dz}{dy})^2}\right) \quad (3)$$

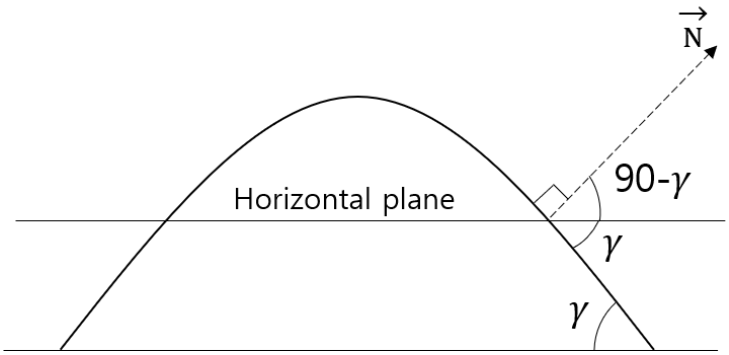

Figure 4. Relationship between slope angle (γ) and normal vector of surface

Aspect angle means a direction of inclination measured from 0°to 360°clockwise with respect to the north of the compass. 90° means eastward and 270° means westward. Gradients direction in the X and Y directions were used to calculate aspect angles. Equation 7 shows aspect angle calculation. The reason for substituting the negative value on the X-axis is that when the forward center difference method was used, the sign of the gradient value in the X-direction is applied in reverse because the gradient direction is reversed. Figure 5 shows the relationship between the 2-arguments arctangent. It appears as a value between 0° and +π and - π based on the x-axis direction

$$Aspect = tan^{-1}\left(\frac{dz}{dy}, -\frac{dz}{dx}\right) \tag{4}$$

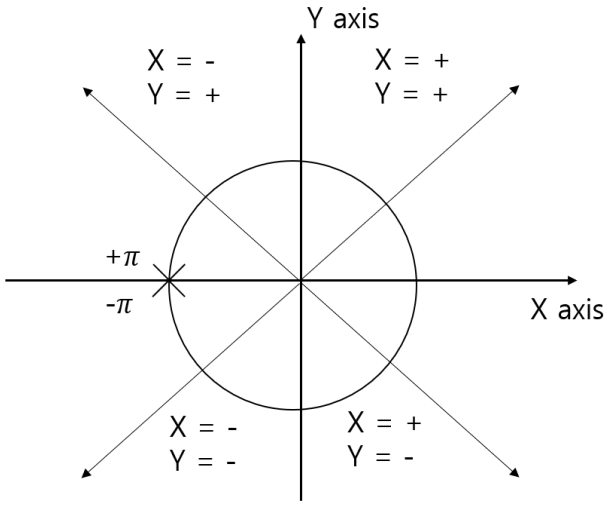

Figure 5. Relationship of 2-arguments arctangent

3.4 Hillshade estimation

The hillshade algorithm is an algorithm that expresses the intensity of illumination through the relationship between the Sun's direction vector and the normal vector on the surface on which the ideal diffuse reflection occurs assuming the Lambertian model (Doumit, 2017; Horn, 1981). The intensity of illumination is calculated through the dot product of the Sun's directional vector and a surface's normal vector. The intensity of illumination varies with the cosine angle. The hillshade algorithm was calculated using slope angle, aspect angle of a surface, the sun's azimuth, and elevation angles at the time of image acquisition. Figure 6 shows a vector on a 3-dimensional coordinate plane of a normal vector and a direction vector of the Sun. In equation (5), α represents the Sun's azimuth angle, and β means the Sun's elevation angle. In equation (6), δ represents the azimuth angle of the surface normal vector, and γ means the slope angle of the surface normal vector. According to Figure 4, the slope on the horizontal plane is at a complementary angle to the slope of the normal vector. Equation (7) is shown as the dot product of two vectors. The smaller the angle between the Sun's direction vector and the normal vector on the surface, the more illumination is received. The larger the angle, the less illumination is received (Konnelly,2002). In addition, Zöppritz (1908) defined it as a shadow when the angle between the light source (I) and the normal vector (SN) is 0 degrees, and it was defined as a shadow when it exceeded 90 degrees.

$$\vec{s} = \begin{bmatrix} \mathrm{x} = \cos\beta \times \cos(90° - \alpha) \\ y = \cos\beta \times \sin(90° - \alpha) \\ z = \sin\beta \end{bmatrix} \tag{5}$$

$$\vec{n} = \begin{bmatrix} \mathrm{x} = \cos(90° - \gamma) \times \cos(90° - \delta) \\ y = \cos(90° - \gamma) \times \sin(90° - \delta) \\ z = \sin(90° - \gamma) \end{bmatrix} \tag{6}$$

$$Hillshade = \vec{s} \cdot \vec{n} = \sin(\beta) \times \sin(90° - \gamma) + \cos(\beta) \times \cos(90° - \gamma) \times \cos(\alpha - \delta)) \tag{7}$$

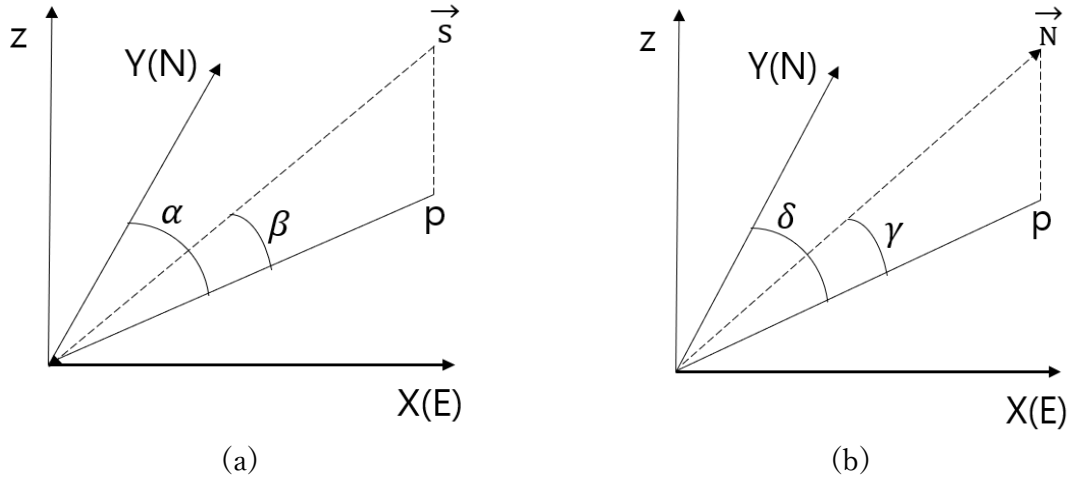

Figure 6. 3-dimensional coordinate system of the Sun's direction Vector (a) and the Earth surface's normal vector (b)

3.5 Verification of accuracy

To evaluate our proposed methods, we used the confusion matrix. This method determines the accuracy of the predicted result by comparing pixels between the truth data and the predicted result. The confusion matrix is shown in Table 2. Recall means the actual positive percentage of what the model classifies as positive. Precision means the ratio of the actual positive data predicted that the model is positive. F1-score is an evaluate indicator with the harmonized average of recall and precision. the higher the F1-socre, the better the performance. Overall accuracy means the percentage of positive in the total samples. Each expression is shown in equation (8) – (11).

Table 2. Confusion Matrix of Predicted Result

		Ground Truth data	
		True	False
Predicted result	True	TP (True Positive)	FP (False Positive)
	False	FN (False Negative)	TN (True Negative)

$$Overall\ Accuracy = \frac{TP+TN}{TP+FN+FP+TN} \tag{8}$$

$$Precision = \frac{TP}{TP+FP} \tag{9}$$

$$Recall = \frac{TP}{TP+FN} \tag{10}$$

$$F1-score = \frac{TP+TN}{TP+FN+FP+TN} \tag{11}$$

4. RESULT

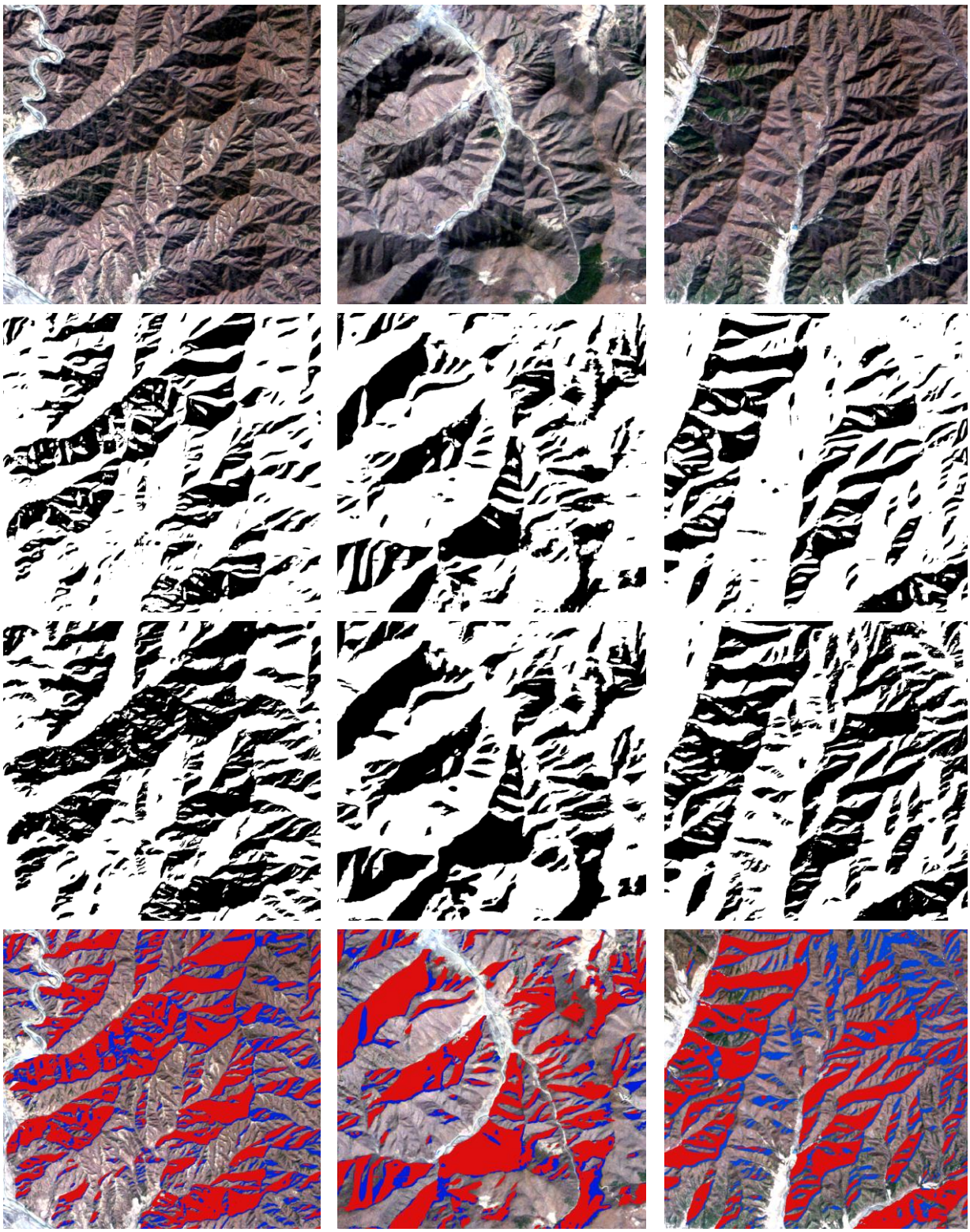

Figure 7. shadow detection result of RapidEye image (from the upper, natural color image, predicted result, ground truth, overlay image of predicted result (red) and ground truth (blue) on natural color image), (a) Hamheung Test Area #A, (b) Hamheung Test Area #B, (c) Hamheung Test Area #C (White is Non-Shadow, Black is Terrain Shadow).

Figure 7 shows the research areas of A, B and C selected for the mountainous region in Hamheung-si. At time of image acquisition, the Sun's azimuth angle was 143.9° and the elevation angle was 42.4°. Image in the first row of Figure 7 are natural color images and images in the second row are the results from the method. Images in the third row are Ground Truth data, and the last row overlaid images of the prediction result and Ground Truth data on the satellite image. In terms of qualitative evaluation, it was confirmed that the shape, location, and size of the shadow seen in the satellite image match in all three regions. Looking at the overlaid image of the prediction results and the Ground Truth data, most of the shadows could be detected, although it was slightly undetected than the Ground Truth data. In the case of A and B areas, the results were similar to the shadow and predicted results by mountain ridges and valleys, however, in the case of C, the slightly bright valleys in the middle of the image were less detected as a shadow. It seemed that undetection was due to the difference in the slope angle and aspect. The mountainous regions include ridges and valleys, and shadows mainly occur in valleys. Our proposed results showed detected shadows at the location of the valley. In addition, a bottom area where the valleys meet is a low and flat area, and shadows are rarely generated. Our predicted results show that those areas have not been detected. And then, the expression of the ridges and valleys was expressed in more detail than the Ground Truth data.

According to a quantitative term, all three regions showed over 85% accuracy. In particular, region B showed more than 90% accuracy. Precision was very high in all three regions. It is determined that there are few misdetections. On the other hand, the reason for the low recall rate seems be the result of the occurrence of many undetected pixels. Consequently, our proposed method has shown that this algorithm can detect terrain shadows with less misdetection.

Table 3. Accuracy table of Predicted Result

Study Area	Ground Truth data							
	TP	TN	FN	FP	Recall	Precision	F1-Score	Overall accuracy
A	322123	652177	148663	9267	0.68	0.97	0.80	0.86
B	298692	630480	83554	1034	0.78	0.99	0.87	0.91
C	269725	593509	145056	6710	0.65	0.97	0.78	0.87

5. CONCLUSIONS

In this study, we proposed a method to detect terrain shadow in RapidEye image by the hillshade algorithm using the surface's normal vector and the Sun's directional vector. Terrain shadows were estimated using only DEM and metadata of satellite images and compared with Truth data. The results showed that result from all test regions have shown satisfactory qualitative and quantitative performances. It was confirmed that our proposed method could be used for terrain shadow detection.

6. ACKNOWLEDGEMENT

This study was conducted as part of the task of the Korea Forest Service's Nation Institute of Forest Science, "Reception, Processing, ARD Standardization, and Development of Intelligent Forest Information Platform (task number: FM0103-2021-01).

REFERENCE

Doumit, J. A. 2017. Digital Terrain Analysis of Lebanon: A Study of Geomorphometry. pp. 25-39.
Horn, B. K. 1981. Hill shading and the reflectance map. Proceedings of the IEEE, 69(1), pp. 14-47.
Konnelly, P. J. 2002. GIS applications to historical cartographic methods to improve the understanding and visualization of contours. Journal of Geoscience Education, 50(4), pp. 428-436.
Li, H., Xu, L., Shen, H., & Zhang, L. 2016. A general variational framework considering cast shadows for the topographic correction of remote sensing imagery. ISPRS Journal of Photogrammetry and Remote Sensing, 117, pp.

161-171.
Lorenzi, L., Melgani, F., & Mercier, G. 2012. A complete processing chain for shadow detection and reconstruction in VHR images. IEEE transactions on geoscience and remote sensing, 50(9), pp. 3440-3452.
Shahtahmassebi, A., Yang, N., Wang, K., Moore, N., & Shen, Z. (2013). Review of shadow detection and de-shadowing methods in remote sensing. Chinese geographical science, 23(4), pp. 403-420.
Tsai, V. J. 2006. A comparative study on shadow compensation of color aerial images in invariant color models. IEEE transactions on geoscience and remote sensing, 44(6), pp. 1661-1671.
Wang, Q., & Yan, L. 2016. ANISOTROPIC SCATTERING SHADOW COMPENSATION METHOD FOR REMOTE SENSING IMAGE WITH CONSIDERATION OF TERRAIN. International Archives of the Photogrammetry, Remote Sensing & Spatial Information Sciences, 41.
Zhang, H., Sun, K., & Li, W. 2014. Object-oriented shadow detection and removal from urban high-resolution remote sensing images. IEEE transactions on geoscience and remote sensing, 52(11), pp. 6972-6982.
Zöppritz, 1908. Leitfaden der Kartenentwurfslehre. In 2. neubearb. und erw. Aufl. hrsg. von Alois Blusau pp. 58-60